Functionalization of Single-Walled Carbon Nanotubes with Well-Defined Polymers by Radical Coupling

Yuanqin Liu, Zhaoling Yao, and Alex Adronov*

Department of Chemistry and the Brockhouse Institute for Materials Research, McMaster University, Hamilton, Ontario L8S 4M1, Canada

Received August 23, 2004; Revised Manuscript Received November 15, 2004

ABSTRACT: Polystyrene and poly[(*tert*-butyl acrylate)-*b*-styrene] with well-defined molecular weights and polydispersities were prepared by nitroxide-mediated free-radical polymerization. The homopolymers and block copolymers were used to functionalize shortened single-walled carbon nanotubes (SWNTs) through a radical coupling reaction involving polymer-centered radicals generated at 125 °C via loss of the stable free-radical nitroxide capping agent. The resulting polymer−SWNT composites were fully characterized and were found to be highly soluble in a variety of organic solvents. This solubility could also be altered through chemical modification of the appended polymers. The *tert*-butyl groups of appended poly[(*tert*-butyl acrylate)-*b*-styrene] could be removed to produce poly[(acrylic acid)-*b*-styrene]-functionalized carbon nanotubes. The resulting composite was found to form aggregates in a mixture of chloroform/methanol (v/v: 1/1) as determined by dynamic light scattering.

Introduction

The potential utility of single-walled carbon nanotubes (SWNTs) in numerous areas, such as molecular wires and electronics,[1] sensors,[2] high-strength fibers,[3] and field emission displays,[4] is now well recognized. However, the inherent insolubility of SWNTs in most organic and aqueous solvents is a major limitation to the solution-phase manipulation and processability of these structures, greatly hindering the widespread application of carbon nanotubes in real devices. Recently, a number of research groups have focused on the chemical functionalization of carbon nanotubes,[5] and it has been demonstrated that appropriate derivatization can increase their solubility. For instance, functionalization of SWNTs with polymers has been shown to drastically affect the solubility of the resulting hybrid materials, closely reflecting the properties of the grafted polymer.[6−13] Many of these approaches have adopted covalent functionalization of carbon nanotubes with polymers, as this ensures close interaction between the two components and precludes phase separation. Recent studies have demonstrated the effectiveness of both "grafting from"[6,7,11,12,14] and "grafting to"[6,9,15−18] approaches to nanotube functionalization. In the "grafing from" method, a higher degree of surface functionalization is possible, but multiple synthetic steps must be carried out on the nanotubes, and polymer characterization is only possible if the grafted chains are cleaved from the nanotube surface.[11,12] Conversely, the "grafting to" method suffers from low theoretical polymer loadings due to steric repulsion between grafted and reacting polymer chains but allows for characterization of polymer chains prior to grafting.[9,15−18] Recent work in our group has investigated the grafting of well-defined polymer architectures to the surface of SWNTs in an attempt to modify their solubility and self-assembly properties. To achieve this goal, the "grafting to" method was favored because it allows for the controlled synthesis and unambiguous characterization of polymer structure prior to the grafting step. We therefore required a method for the synthesis of architecturally well-defined polymer structures that would also enable subsequent attachment of the synthesized polymers to the nanotube walls.

We decided to build upon the previously described radical functionalization methods which have emerged from the pioneering work with C_{60} by Krusic and coworkers.[19,20] These studies have shown that radical species can efficiently couple to the surface of C_{60}, resulting in highly functionalized fullerenes. Similar reactions have also been extended to nanotubes, where the coupling of a variety of organic radicals has been shown to improve nanotube solubility.[21,22] Addition of macromolecules to these structures has also been demonstrated using free radical polymerization, where termination was shown to occur by coupling to both fullerenes and nanotubes.[23,24] Functionalization of fullerenes with well-defined polymers, produced by atom transfer radical polymerization (ATRP), has also been recently described.[25−27] Over the past decade, advances in nitroxide-mediated radical polymerization (NMP) have demonstrated the feasibility of this technique for the polymerization of numerous monomers and the preparation of complex polymer architectures.[28−31] Considering that NMP produces well-defined polymers that are end-capped with thermally labile nitroxide functionalities, it was postulated that this method could result in the controlled formation of polymer-centered radicals that could be utilized in the functionalization of SWNTs, similar to what has been shown with C_{60}.[25] Here, we describe the use of NMP to prepare well-defined, narrow polydispersity homopolymers and diblock copolymers, followed by their attachment to the surface of SWNTs using a facile and efficient radical coupling reaction. This reaction simply requires the synthesized polymers to be heated to 125 °C in the presence of SWNTs. We have found that the resulting polymer−nanotube conjugates exhibit a high solubility in various organic solvents, which can be altered by chemical modification of the polymers.

Results and Discussion

Functionalization of Shortened SWNTs with Polystyrene. Nitroxide-terminated polystyrene (PS)

* Corresponding author: e-mail adronov@mcmaster.ca; Tel (905) 525-9140 x23514; Fax (905) 521-2773.

10.1021/ma048273s CCC: $30.25 © 2005 American Chemical Society
Published on Web 01/20/2005

Scheme 1. Preparation of PS by Nitroxide-Mediated "Living" Free-Radical Polymerization and Its Utilization for the Functionalization of SWNTs

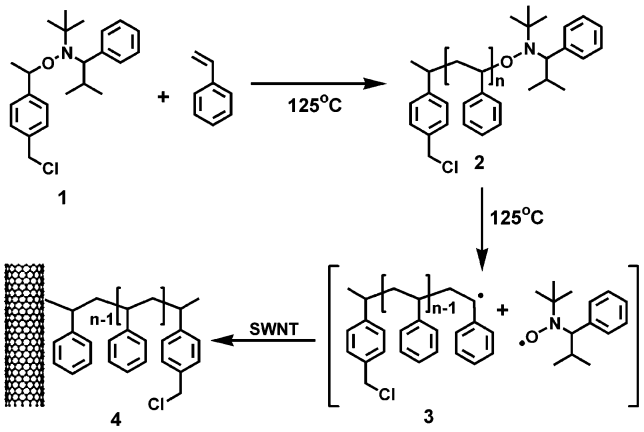

samples were prepared by "living" free-radical polymerization utilizing one of the universal alkoxyamine unimolecular initiators recently introduced by Hawker and co-workers (Scheme 1).[32] Following standard polymerization procedures,[32] a sample of PS having a molecular weight of 4900 g/mol and a polydispersity of 1.09 was prepared. (The sample was analyzed by size exclusion chromatography, measured against commercial PS standards.) The SWNTs used in this study, produced by the HiPco process, were purchased from Carbon Nanotechnologies, Inc. We chose to shorten the as-received nanotubes by sonication in a mixture of HNO_3/H_2SO_4 to lengths of ca. 330 nm to enhance the solubility of our desired nanotube−polymer conjugates.[11]

The radical addition of PS to shortened SWNTs (Scheme 1) was done by dispersing 10 mg of the SWNTs in anhydrous DMF (15 mL) and then adding the nitroxide-terminated PS (500 mg) along with a catalytic amount of acetic anhydride (50 μL) in order to activate the nitroxide end group toward homolytic cleavage.[33] After bubbling with N_2 for 30 min, the mixture was immersed in a 125 °C oil bath and stirred under Ar for 3 days. Upon cooling, the reaction mixture was filtered through a 200 nm pore-diameter Teflon membrane and washed with large quantities of THF and CH_2Cl_2 (200 mL each) to remove any unreacted PS. The residual black solid was peeled away from the Teflon membrane and was dried at 50 °C under vacuum overnight. It was found that the functionalization reaction drastically affected the solubility characteristics of the resulting material. As illustrated in Figure 1A, the initial shortened SWNTs exhibit some solubility in water prior to polymer functionalization. However, after functionalization with PS, the composite (**4**) lost its solubility in H_2O and became highly soluble in a range of organic solvents, including CH_2Cl_2, THF, $CHCl_3$, and toluene (Figure 1B−D). This high solubility allowed us to confirm the absence of any free polymer within our sample by simple thin-layer chromatography (TLC), through which we could observe a baseline spot corresponding to our nanotube conjugates and a complete lack of any spots corresponding to free polymer, which would appear near the solvent front when using CH_2Cl_2 as the eluent. A control experiment, in which nanotubes were mixed with the same nitroxide-terminated polymers at room temperature instead of 125 °C, was also performed. Under these conditions, the nitroxide end group is stable and polymeric radicals are not

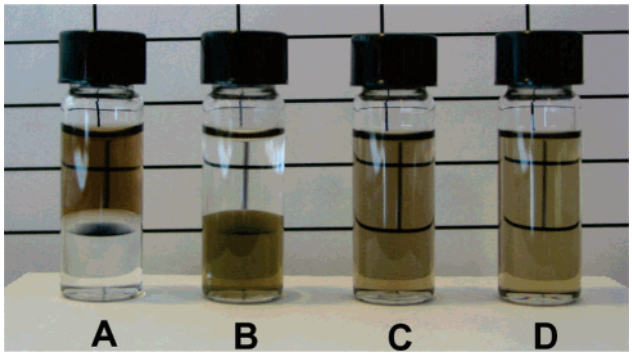

Figure 1. Solutions of SWNT samples in various solvents: (A) shortened SWNTs in CH_2Cl_2/H_2O; (B) PS-functionalized SWNTs in CH_2Cl_2/H_2O; (C) PS-functionalized SWNTs in THF; (D) PS-functionalized SWNTs in $CHCl_3$.

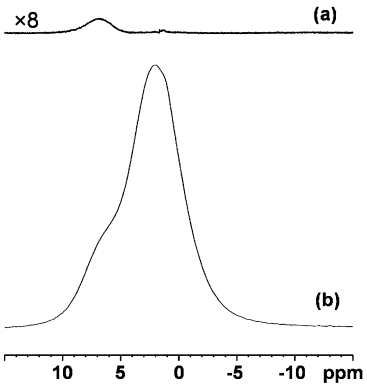

Figure 2. Solid-state NMR spectra of (a) shortened unfunctionalized SWNTs and (b) initiator-functionalized SWNTs.

expected to be produced. Filtration and washing using the same protocol as outlined above resulted in complete removal of the free polymer from the nanotube residue, as indicated by an absence of a mass increase and a complete lack of nanotube solubility in organic solvents. A further control experiment, in which the SWNTs were reacted with the alkoxyamine initiator (**1**) alone, under identical conditions and concentrations to the polymer reactions described above, resulted in no increase in the solubility of the resulting SWNTs. In this case, magic-angle spinning solid-state NMR provided some evidence that functionalization of the SWNTs with initiator fragments did occur (Figure 2), but these structures were too small to impart any solubility difference to the SWNTs. For reference, the spectrum of shortened, unfunctionalized nanotubes is also shown and only exhibits a very weak signal due to the presence of acid groups at the ends and defect sites of the nanotubes, introduced as a result of the shortening process.

The degree of SWNT solubility in various solvents as a result of functionalization could be estimated by UV/vis spectroscopy following a procedure published by Smalley and Tour, who reported the specific extinction coefficient for HiPco SWNTs at 500 nm to be 0.028.[34] We also measured the specific extinction coefficient of our shortened, polymer-functionalized SWNTs to determine whether the shortening and functionalization process has an effect on their absorption properties. Three separate samples of polymer-functionalized SWNTs **4** were dissolved in 10 mL of THF and allowed to stand overnight to enable any insoluble material to settle. The supernatant from each of these solutions was diluted five times to produce a total of 15 different samples of varying concentration (see Experimental

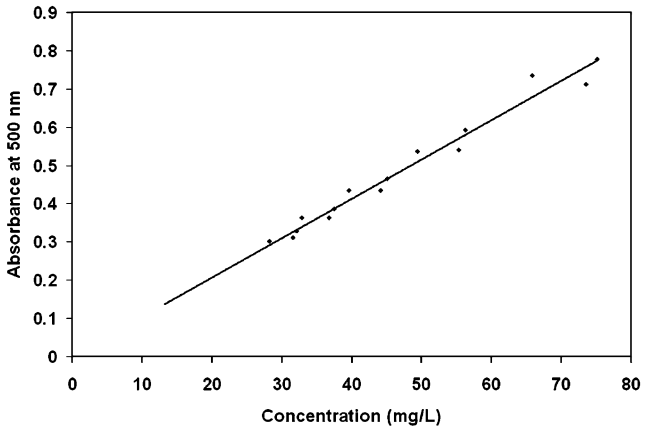

Figure 3. Optical density at 500 nm of shortened SWNTs in THF at different concentrations. The straight line is a linear least-squares fit to the data having a slope of 0.0103.

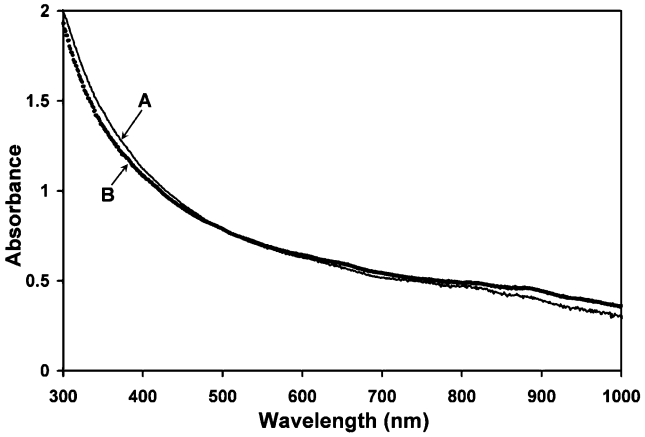

Figure 4. UV/vis spectra of (A) shortened SWNTs in H_2O and (B) PS-functionalized SWNTs in THF (normalized for absorption at 500 nm).

Section). The absorption spectrum of each of these solutions was then measured, and the absorption value at 500 nm was plotted against nanotube concentration. Thermogravimetric analysis (TGA) was employed to determine the weight percent of nanotubes within the polymer-functionalized materials, allowing the calculation of the exact amounts of nanotubes present within the dissolved material used in the absorption experiment. Therefore, the slope of the linear least-squares fit of the plotted data provided the specific extinction coefficient for the functionalized nanotubes within our sample (Figure 3). This specific extinction coefficient was found to be 0.0103, with an *R*-squared value of 0.974, and can be used to estimate the concentration of nanotube solutions. Our measured specific extinction coefficient is significantly lower than that reported by Smalley and Tour, indicating that shortened, polymer-functionalized nanotubes are less efficient absorbers of light than pristine, full-length nanotubes. This value was used to determine the maximum concentration of the polymer-functionalized nanotube sample in various organic solvents. The highest solubility was found to be in THF, with a nanotube concentration in excess of 600 mg/L. Figure 4 shows the UV/vis absorbance of PS−SWNTs in THF (curve B), which is very similar to the spectrum of shortened, unfunctionalized SWNTs (curve A).

Because of this relatively high solubility, solution-phase ^{1}H NMR spectroscopy could be utilized to study the polymer portion of the sample. Figure 5 depicts the

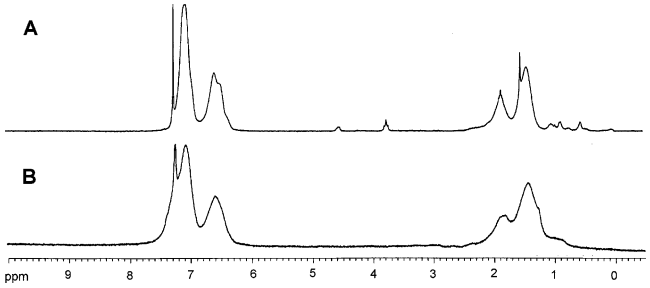

Figure 5. ^{1}H NMR spectra of (A) PS and (B) PS-functionalized SWNTs.

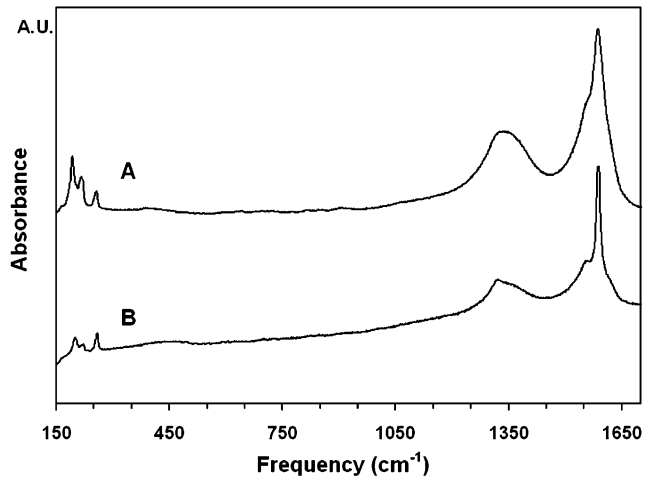

Figure 6. Raman spectra of (A) shortened SWNTs and (B) PS-functionalized SWNTs, measured on solid powders with an excitation wavelength of 632.8 nm.

^{1}H NMR spectra of the PS sample used in nanotube functionalization and the PS-functionalized SWNTs (**4**). The two spectra are nearly identical, clearly illustrating that PS was, indeed, attached to the surface of carbon nanotubes. Both of the spectra show the expected aromatic signals for PS at $\delta = 7.07$ and 6.56 ppm (broad) as well as the backbone signals at $\delta = 1.84$ and 1.42 ppm. The relatively small peaks below 1.0 ppm in Figure 5A are due to the alkoxyamine initiator fragments at the ends of the polymer chains. These signals remain after functionalization (Figure 5B), indicating that some nitroxide radical fragments may have also coupled to the SWNTs during the course of the reaction.

The PS−SWNT composite and shortened SWNTs were additionally analyzed by Raman spectroscopy, and both exhibited the characteristic nanotube absorptions at ca. 190−260 and 1550−1590 cm^{-1}, corresponding to the radial breathing modes (RBM) and the tangential G mode of the SWNTs, respectively (Figure 6). Previous studies have shown that the observed RBM frequencies are inversely proportional to nanotube diameter,[35,36] allowing the determination of nanotube diameter distributions within samples. Interestingly, after functionalization, we observed a decrease in the intensity of the lower frequency RBM absorptions, indicating a decrease in the amount of larger diameter nanotubes in the sample. This implies that smaller diameter nanotubes may be more reactive toward the radical coupling reaction. It should be noted that the PS−SWNT samples used for Raman analysis were obtained by evaporating the decanted supernatant of concentrated solutions that were allowed to settle for at least 1 day. These samples were therefore free of any insoluble, presumably unfunctionalized portions of the material. Others have also

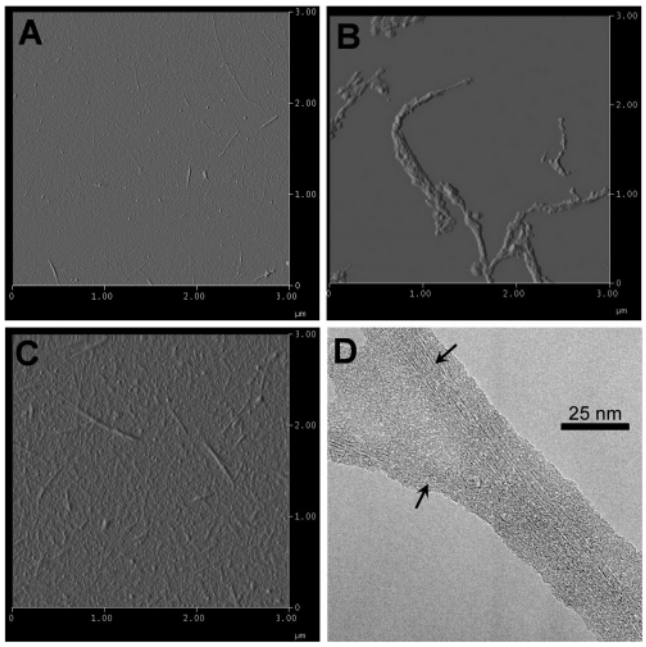

Figure 7. (A) AFM image of purified SWNTs. (B) AFM image of PS-functionalized SWNTs spun-cast from THF solution. (C) AFM image of PS-functionalized SWNTs spun-cast from $CHCl_3$ solution. (D) TEM image of PS-functionlized SWNTs with arrows indicating some locations of nanotubes.

observed diameter-selective reactivity in both sidewall and defect-site functionalization reactions,[37,38] attributing the higher reactivity of lower diameter tubes to π-orbital misalignment and pyramidalization strain energy, both of which are inversely proportional to tube diameter.[39] Differences in the tangential G mode before and after the radical functionalization can also be seen from the Raman data. Here, the diameter-dependent Breit−Wigner−Fano (BWF) peak,[40] seen as a close shoulder to the higher frequency, diameter-independent Lorentzian peak at 1585 cm^{-1} prior to functionalization (Figure 6A), shifts to lower frequency after functionalization (Figure 6B). This shift is consistent with previous observations of direct proportionality between the frequency of the BWF peak and nanotube diameter.[40] Again, this lends evidence to the fact that the radical coupling reaction is selective for lower diameter nanotubes. Finally, the broad disorder peak at approximately 1320 cm^{-1} is present in both spectra and corresponds to sp^3-hybridized carbon atoms at defect sites within the nanotubes. The relative intensity of this peak seems to decrease after polymer functionalization, but the exact cause of this decrease in the number of sp^3-hybridized carbon atoms within the lower diameter nanotubes is unknown. Overall, the Raman results indicate that, although the nanotube solubility has increased dramatically as a result of functionalization, the chemical structure of the SWNTs has mainly been preserved.

Atomic force microscopy (AFM) analysis of the PS-functionalized SWNTs revealed that the topological morphology of these materials is significantly altered when compared to unfunctionalized SWNTs. Figure 7A depicts a sample of shortened SWNTs prior to functionalization, prepared by spin-casting from a DMF suspension onto freshly cleaved mica, where small nanotube bundles having heights in the range of 1−5 nm can be observed. After polymer functionalization, the nanotube sample was spun-cast from a THF solution, again onto freshly cleaved mica, and revealed nanotube bundles

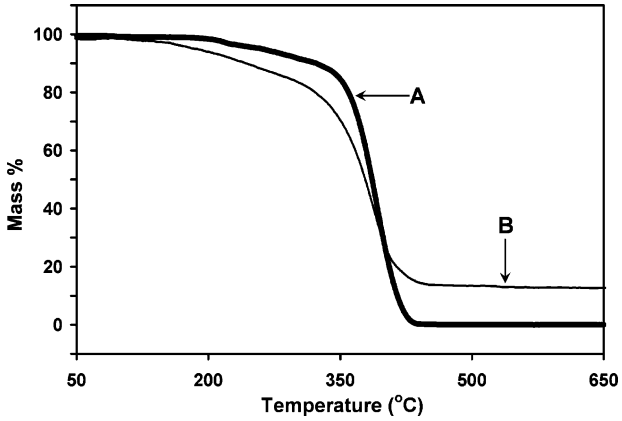

Figure 8. TGA traces of (A) PS and (B) PS-functionalized SWNTs.

that were coated or closely associated with an amorphous material, presumably PS (Figure 7B). In this sample, individual features reached heights of up to 15 nm, and the overall dimensions of these polymer-functionalized structures indicate the formation of aggregates, possibly due to polymer entanglement. Interestingly, changing the casting solvent to $CHCl_3$ resulted in a completely different surface topology, where the nanotube bundles seemed to be embedded in a polymeric matrix (Figure 7C). This is likely due to polymer chains extending away from SWNTs on the surface, rather than coiling around the polymer, as in Figure 7B. It is presumed that differences in the nanotube−polymer vs nanotube−solvent interactions are responsible for the observed topological changes, since SWNTs have been shown to be more soluble in $CHCl_3$ than in THF.[34] This implies that nanotube−solvent interactions are stronger in chloroform, making it more favorable for polymers to extend out into solution and therefore expose the nanotubes. Upon spin-coating such a solution, these extended polymer conformations become immobilized on the surface and lead to the observed morphologies. TEM analysis of the PS-functionalized structures also revealed the presence of SWNTs coated with amorphous polymeric material (Figure 7D). Here, the high resolution of the TEM allows observation of the individual nanotubes, along with surrounding amorphous polymer, within a polymer-functionalized bundle.

The polymer-functionalized SWNTs were also studied by thermogravimetric analysis (TGA). The TGA traces for both the starting PS and the grafted nanotubes are shown in Figure 8. The PS sample completely decomposes in the temperature range between 365 and 450 °C. Although the PS-functionalized nanotube sample exhibits a very similar decomposition curve, the mass loss stops at approximately 13% and remains stable to 800 °C, indicating that the sample was composed of 13% nanotubes by weight. Interestingly, the onset of decomposition in the nanotube sample is at slightly lower temperature, possibly due to the high thermal conductivity of the SWNTs in the sample.

Functionalization of Shortened SWNTs with Diblock Copolymers. Taking advantage of the synthetic control provided by nitroxide-mediated radical polymerization, we were able to prepare a diblock copolymer composed of a poly(*tert*-butyl acrylate) block and a polystyrene block (PtBA-*b*-PS), as depicted in Scheme 2. Similar approaches using atom transfer radical polymerization have been described recently.[41] The resulting diblock copolymer **6** had a molecular

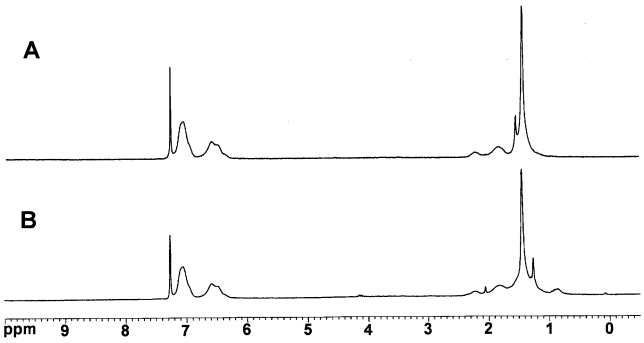

Figure 9. ^{1}H NMR spectra of (A) PtBA-*b*-PS and (B) PtBA-*b*-PS-functionalized SWNTs.

Scheme 2. Preparation of PtBA-*b*-PS by Nitroxide-Mediated "Living" Free-Radical Polymerization and Its Utilization for the Functionalization of SWNTs

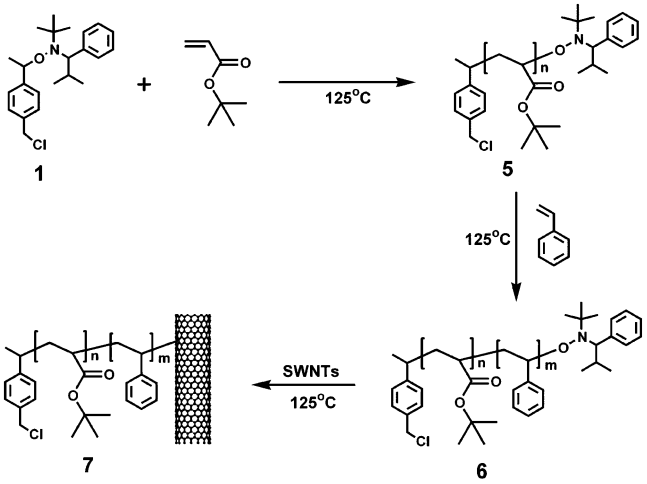

weight of 18 000 g/mol and a PDI of 1.40, determined by SEC against polystyrene standards. ^{1}H NMR indicated that the monomer ratio of tBA to styrene in the product was approximately 1:2.5. Coupling of the polystyrene block to shortened SWNTs was performed according to the aforementioned procedure at 125 °C and resulted in block copolymer-functionalized SWNTs **7** (Scheme 2).

The block copolymer-functionalized SWNTs were also found to be highly soluble in various organic solvents, including THF, CH_2Cl_2, and $CHCl_3$, with concentrations of SWNTs exceeding 200 mg/L (based on the calculated specific extinction coefficient from Figure 3). Comparing the solution ^{1}H NMR spectra of the block copolymer and the copolymer-functionalized SWNTs (Figure 9), it is clear that the two spectra are nearly identical. Considering that any free polymer can easily be removed by filtration and its absence can be determined by TLC, the similarity of these NMR spectra is indicative of nanotube functionalization with the block copolymer.

TGA analysis also confirmed that the block copolymer functionalization had occurred. Figure 10 illustrates the TGA traces for the bulk PtBA-*b*-PS (i) and the PtBA-*b*-PS-functionalized SWNTs (ii). For this block copolymer, two decomposition events are clearly visible, with the first one at ca. 200 °C attributed to the loss of the *tert*-butyl groups in the PtBA block (~25% mass loss) and the second being the depolymerization of the remaining polymer. The nanotube-attached polymer decomposes in a virtually identical manner, again

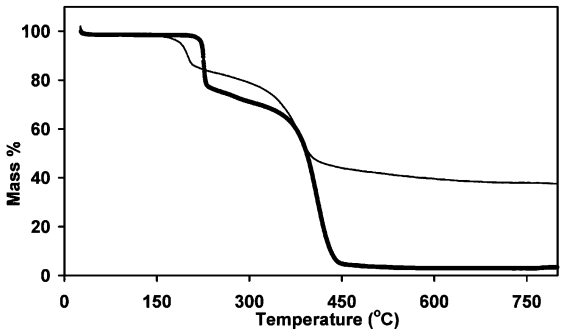

Figure 10. TGA data for PtBA-*b*-PS (i) and PtBA-*b*-PS-functionalized SWNTs (ii).

Scheme 3. Deprotection of PtBA-*b*-PS-Functionalized SWNTs To Produce PAA-*b*-PS-Functionalized SWNTs

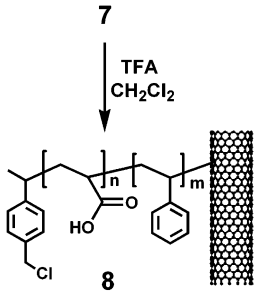

confirming its composition, but does not reach a complete mass loss above 450 °C. The remaining mass, approximately 38%, gives an indication of the nanotube content in the original sample. Clearly, the relatively high nanotube content in this sample, as compared to the polystyrene-functionalized sample (**4**), indicates that the functionalization step was less efficient and also partly explains the decreased solubility of this material. Again, this sample exhibits a slightly decreased onset of decomposition for both steps, similar to what was observed for the homopolymer (Figure 8). This phenomenon may be due to the increased thermal conductivity imparted to the material due to the presence of SWNTs.

SWNTs Functionalized with Amphiphilic Block Copolymers. We have previously shown that removal of the *tert*-butyl groups of poly(*tert*-butyl acrylate)-functionalized SWNTs drastically affects their solubility properties.[11] Along similar lines, the *tert*-butyl groups within the nanotube-attached PtBA-*b*-PS polymer could be removed by treating the sample with a 20% trifluoroacetic acid (TFA)/CH_2Cl_2 solution (v/v) for 12 h (Scheme 3). Upon evaporation of the solvent and acid, the resulting poly(acrylic acid)-*block*-polystyrene (PAA-*b*-PS)-functionalized SWNTs (**8**) were found to be completely insoluble in organic solvents such as THF and CH_2Cl_2 but also insoluble in pure H_2O and CH_3OH. However, this sample was soluble in mixtures of chloroform and methanol of various composition. Interestingly, changes in polymer morphology as a result of changing the solvent composition could be observed. For example, Figure 11A depicts the ^{1}H NMR spectrum of the PAA-*b*-PS-functionalized SWNT solution in a 3/1 mixture of $CDCl_3/CD_3OD$ (v/v), where both the acrylic acid and styrene blocks dissolve very well. The broad aromatic signals for the styrene block are clearly visible at $\delta = 6.91$ and 6.43 ppm. Aliphatic proton signals were also observed in the region between 0.8 and 2.3 ppm, corresponding to the polymer backbone protons for both blocks. The signals at $\delta = 1.69$ and 3.56 ppm are due to traces of THF left from the deprotection process that

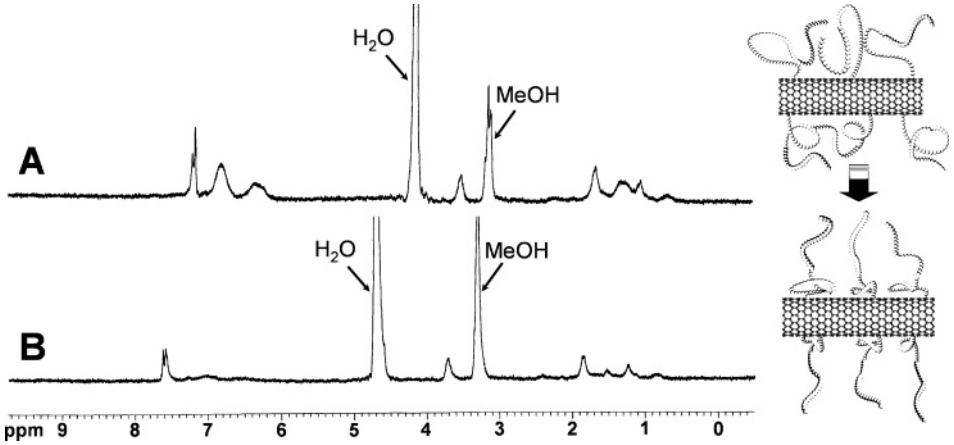

Figure 11. Solution ^{1}H NMR spectra of (A) PAA-*b*-PS-functionalized SWNTs in $CDCl_3/CD_3OD$ (v/v: 3/1) and (B) PAA-*b*-PS-functionalized SWNTs in $CDCl_3/CD_3OD$ (v/v: 1/1).

were difficult to remove, even after prolonged heating under vacuum. When the deuterated methanol portion of the solvent was increased to a $CDCl_3/CD_3OD$ ratio of 1:1, the ^{1}H NMR of the sample exhibited significant changes (Figure 11B). In this case, both the aromatic and aliphatic signals corresponding to the PS block dramatically decreased in intensity, while the signals corresponding to the PAA block remained practically unchanged. This behavior is indicative of a contraction and rigidification of the PS block (Figure 11, cartoon), making it less mobile and thereby dramatically increasing the relaxation time of the protons associated with it. It should be noted that this behavior is completely reversible, where evaporation of the solvent and reuptake in a 3/1 $CDCl_3/CD_3OD$ mixture reproduces the ^{1}H NMR trace shown in Figure 11A.

Dynamic light scattering (DLS) was also utilized to determine the size distributions of the block copolymer-functionalized SWNTs. In the case of the nanotubes functionalized with the amphiphilic block copolymer, the observed diameter of the material was again found to vary with solvent composition. Starting with the relatively nonpolar solvent mixture containing 6/1 $CHCl_3$/MeOH, the light scattering measurement indicated a hydrodynamic diameter of 164 nm. Considering that the average length of the nanotubes, as measured by AFM, is approximately 330 nm, the DLS data seem to indicate that, in solution, the polymer-functionalized nanotubes are still flexible enough to fold and adopt shapes that are more compact than would be expected from fully elongated structures. However, rodlike molecules with high aspect ratios are not ideal for light scattering measurements, and the absolute values obtained by this method may not be meaningful. Interestingly, as the solvent composition was increased in polarity to a 1/1 and 1/2 $CHCl_3$/MeOH ratio, the measured hydrodynamic diameter increased to 302 and 712 nm, respectively (Figure 12). These data, along with the solution ^{1}H NMR data, are consistent with a contraction and rigidification of the polystyrene block, which may result in micelle-like behavior where the polar PAA segments stabilize SWNT aggregates. In the more polar solvent, multiple SWNTs with closely associated PS likely form a hydrophobic "core" that is surrounded and stabilized by PAA chains.

Conclusions

Nitroxide-mediated polymerization was used to prepare a series of well-defined polymers that varied in length and composition. These polymers were covalently attached to SWNTs through thermolytic release of the nitroxide end groups in the presence of SWNTs, which led to an efficient radical coupling of the polymers to the nanotube sidewalls. The resulting polymer-functionalized nanotubes were highly soluble in a range of organic solvents, and this solubility could be controlled by varying the chemical composition of the appended polymers. Amphiphilic block copolymers were also coupled to SWNTs, and solution NMR and light scattering data indicated that it is possible to induce changes in polymer morphology, and possibly nanotube aggregation, by varying solvent composition. The high solubility and environmental responsiveness of these materials may impact the future technological applicability of carbon nanotubes.

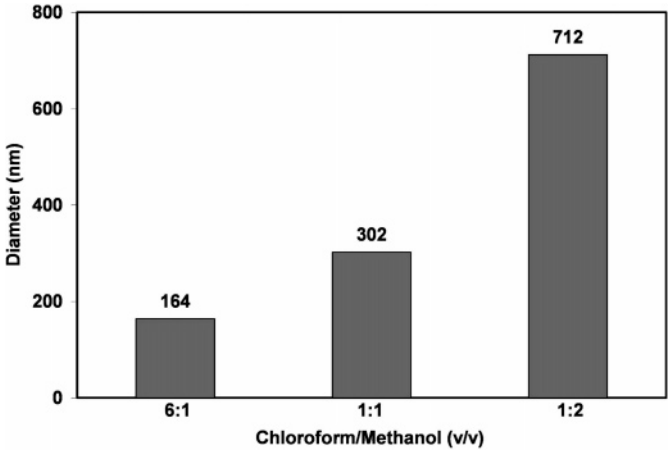

Figure 12. DLS data for PAA-*b*-PS-functionalized SWNTs in various $CHCl_3$/MeOH solvent compositions.

Experimental Section

General. Single-walled carbon nanotubes (SWNTs) were purchased from Carbon Nanotechnologies, Inc. (Houston, TX). Styrene and *tert*-butyl acrylate were purified by passing through basic alumina and stored in the fridge. All other reagents and solvents were purchased from commercial suppliers and used as received. Raman spectra were obtained using a Renishaw InVia Raman microscope equipped with an 1800 grooves/mm grating and a CCD detector, with excitation at 632.8 nm from a He−Ne laser typically operated at a laser power of 6 mW (although some samples were measured at 3 mW to reduce noise due to sample fluorescence). Samples were prepared by evaporating the supernatant of concentrated solutions and thoroughly drying the resulting solid powders.

These powders were then placed in glass vials and were measured using a 60 s accumulation time. Atomic force microscopy was done using a Digital Instruments NanoScope IIIa Multimode AFM, with samples prepared by spin-coating sample solutions or suspensions on freshly cleaved mica substrates. The images were recorded with standard tips in tapping mode at a scan rate of 1.0 Hz. TEM analysis was performed using a Philips CM12 operating at 120 keV. Solution NMR was performed on a Bruker 200 MHz instrument in $CDCl_3$. Solid-state ^1H MAS NMR experiments were performed on a Bruker DRX 500 spectrometer, under conditions that were previously described.[42] Filtration was done through either a 100 nm pore polycarbonate membrane (Millipore) or a 200 nm pore Teflon membrane (Millipore). Polymer molecular weight and polydispersity index (PDI) were estimated by gel permeation chromatography (GPC) using a Waters 2695 separations module equipped with a Waters 2996 photodiode array detector, a Waters 2414 refractive index detector, a Waters 2475 Multi λ fluorescence detector, and four Polymer Labs PLgel individual pore size columns. Polystyrene standards were used for calibration, and tetrahydrofuran (THF) was used as the eluent at a flow rate of 1.0 mL/min. Differential scanning calorimetry (DSC) was performed on a TA 2100 modulated differential scanning calorimeter with a temperature gradient of 15 deg/min. The concentrations of the soluble polymer-functionalized SWNTs were calculated from UV/vis absorption spectra measured using a Cary 50 UV/vis spectrophotometer. Thermogravimetric analysis (TGA) was carried out on a NETZSCH STA 409 PC instrument under Ar with a temperature range from 20 to 800 °C and a temperature gradient of 5 deg/min. Particle sizing was conducted by dynamic light scattering. A Lexel 95 ion laser operating at a wavelength of 514 nm was used as the light source, and data were analyzed using a BI-9000AT digital autocorrelator, version 6.1 (Brookhaven Instruments Corp.). The light scattering was measured at 90°.

Shortening and Purification of SWNTs. A 250 mL flask charged with SWNTs (100 mg) and a H_2SO_4/HNO_3 (v/v: 3/1) (120 mL) solution was sonicated for 2 h. Then the suspension was diluted in a 1000 mL beaker with distilled water (800 mL). *Extreme caution must be used when adding water to concentrated acid!* After cooling to room temperature, the dilute solution was filtered through a 100 nm pore diameter polycarbonate membrane. The black material collected on the membrane was added to a 250 mL flask and stirred with H_2SO_4/H_2O_2 (v/v: 9/1, 50 mL) for 30 min at room temperature. Another 50 mL of H_2SO_4/ H_2O_2 (v/v: 9/1) was added, and the suspension was sonicated for 5 min. After dilution using distilled water (800 mL) in a 1000 mL beaker, the suspension was filtered again. The SWNT mat was washed thoroughly using NaOH solution (10 mmol, 250 mL) and distilled water until the pH of the filtrate was 7. Then the nanotubes were washed with an HCl solution (2.0 M, 50 mL) before drying under vacuum overnight. The product was obtained as a black solid (70 mg, 70% yield). IR (KBr pellet): ν = 1748 (m), 1632 (m).

Synthesis of Polystyrene (2). A 25 mL round-bottom flask was charged with styrene (4.0 mL, 35.0 mmol), alkoxyamine initiator (**1**) (288 mg, 0.77 mmol), and acetic anhydride (0.03 mL, 0.32 mmol). The mixture was bubbled with N_2 for 30 min, and then the flask was placed into a 125 °C oil bath. The reaction was allowed to proceed for 12 h, and the product was dissolved in CH_2Cl_2 and then precipitated by dropwise addition of the solution into methanol. The precipitate was filtered and then dried at 50 °C under vacuum overnight. The product was analyzed by GPC (M_n = 4900, PDI = 1.09). ^1H NMR (200 MHz, $CDCl_3$): δ 7.08 (broad), 6.59 (broad), 1.90 (broad), and 1.49 ppm (broad).

Synthesis of Polystyrene-Functionalized SWNTs (4). 10 mg of purified SWNTs, 0.05 mL (0.53 mmol) of acetic anhydride, and 500 mg of polystyrene (M_n = 4900 g/mol) were dispersed in 15 mL of DMF in a 50 mL flask. The mixture was bubbled with N_2 for 30 min and then was stirred at 125 °C under argon for 3 days. The product was collected by filtering through a 200 nm pore Teflon membrane while washing thoroughly with CH_2Cl_2, THF, and methanol and then dried under vacuum overnight. ^1H NMR (200 MHz, $CDCl_3$): δ 7.08 (broad), 6.60 (broad), 1.80 (broad), and 1.43 ppm (broad).

Measurement of the Specific Extinction Coefficient. Three separate samples of polymer-functionalized SWNTs (**4**), weighing 12.1, 11.6, and 10.2 mg, were placed in vials followed by addition of 10 mL aliquots of THF to each sample. The three vials were sonicated for 1 min and then allowed to stand undisturbed overnight. The supernatant of each vial was carefully separated, leaving a small amount of insoluble residue. This residue was dried in a vacuum oven at 50 °C until constant weight (2 h), and the mass of the residue was measured (2.3, 2.6, and 1.5 mg, respectively), allowing for correction of the soluble sample concentrations. Subsequently, 1 mL of each supernatant was placed into five separate vials and diluted with 2−6 mL of THF prior to the UV/vis absorption measurement. Thermogravimetric analysis provided the weight percentage of nanotubes within the polymer-functionalized materials, allowing the calculation of nanotube concentration within the measured solutions.

Synthesis of Poly(*tert*-butyl acrylate) (5). A 25 mL round-bottom flask was charged with *tert*-butyl acrylate (3.0 mL, 20.4 mmol), alkoxyamine initiator (**1**) (176 mg, 0.47 mmol), acetic anhydride (0.05 mL, 0.53 mmol), and chlorobenzene (2.0 mL). The mixture was bubbled with N_2 for 30 min, and then the flask was placed into a 125 °C oil bath. The reaction was allowed to proceed for 12 h, and the product was dissolved in THF and then precipitated by dropwise addition of the solution into methanol/H_2O (v/v: 1/1). The precipitate was filtered and then dried at 50 °C under vacuum overnight. The product was analyzed by GPC, resulting in a M_n = 5900 g/mol and a PDI = 1.62. ^1H NMR (200 MHz, $CDCl_3$): δ 2.21 (broad), 1.82 (broad), and 1.42 ppm (broad).

Synthesis of Poly[(*tert*-butyl acrylate)-*b*-styrene] (6). A 25 mL round-bottom flask was charged with styrene (3 mL, 26.0 mmol), 1.5 g of poly(*tert*-butyl acrylate) (M_n = 5900 g/mol), acetic anhydride (0.05 mL, 0.53 mmol), and chlorobenzene (3.0 mL). The mixture was bubbled with N_2 for 30 min, and then the flask was placed into a 125 °C oil bath. The reaction was allowed to proceed for 12 h, and the product was dissolved in THF and then precipitated by dropwise addition of the solution into methanol. The precipitate was filtered and then dried at 50 °C under vacuum overnight. The product was analyzed by GPC, resulting in a M_n = 18 200 g/mol and a PDI = 1.40. ^1H NMR (200 MHz, $CDCl_3$): δ 7.03 (broad), 6.56 (broad), 2.20 (broad), 1.82 (broad), and 1.42 ppm (broad).

Synthesis of Poly[(*tert*-butyl acrylate)-*b*-styrene]-Functionalized SWNTs (7). 10 mg of purified SWNTs, 0.05 mL (0.53 mmol) of acetic anhydride, and 500 mg of PtBA-*b*-PS (M_n = 18 226 g/mol) were dispersed in 15 mL of DMF in a 50 mL flask. The mixture was bubbled with N_2 for 30 min and then was stirred at 125 °C under argon for 3 days. The product was collected by filtering through a 200 nm pore Teflon membrane while washing thoroughly with CH_2Cl_2, THF, and methanol and then dried at 50 °C under vacuum overnight. The mass of the isolated product increased by approximately 50%. ^1H NMR (200 MHz, $CDCl_3$): δ 7.05 (broad), 6.58 (broad), 2.20 (broad), 1.82 (broad), 1.44 (broad), and 0.88 ppm (broad).

Formation of Poly(acrylic acid-*b*-styrene)-Functionalized SWNTs (8). 8.0 mg of PtBA-*b*-PS-functionalized SWNTs, 1.0 mL of trifluoroacetic acid (TFA), and 5.0 mL of CH_2Cl_2 were dispersed in 15 mL of DMF in a 25 mL flask. The mixture was stirred at room temperature for 6 h. Then the solvent and excess TFA were evaporated in vacuo. The product was dried at 50 °C under vacuum overnight. ^1H NMR (200 MHz, $CDCl_3$/CD_3OD (v/v: 3/1)): δ 6.91 (broad), 6.43 (broad), 2.22 (broad), 1.70 (broad), 1.30 (broad), 1.09 (broad), and 0.71 ppm (broad).

Acknowledgment. This work was supported by grants from the Natural Science and Engineering Research Council of Canada (NSERC), Materials and Manufacturing Ontario (Emerging Materials Knowledge Program), as well as McMaster University. Additionally, we thank Prof. A. Vreugdenhil for Raman spectroscopy

data, Prof. Gianluigi A. Botton and Mr. Travis Casagrande for TEM data, and Prof. Gillian Goward and Ms. Lindsey Cahill for solid-state MAS−NMR data.

References and Notes

(1) Avouris, P. *Acc. Chem. Res.* **2002**, *35*, 1026−1034.
(2) Dai, H. J. *Acc. Chem. Res.* **2002**, *35*, 1035−1044.
(3) Ajayan, P. M. *Chem. Rev.* **1999**, *99*, 1787−1799.
(4) Choi, W. B.; Chung, D. S.; Kang, J. H.; Kim, H. Y.; Jin, Y. W.; Han, I. T.; Lee, Y. H.; Jung, J. E.; Lee, N. S.; Park, G. S.; Kim, J. M. *Appl. Phys. Lett.* **1999**, *75*, 3129−3131.
(5) Hirsch, A. *Angew. Chem., Int. Ed.* **2002**, *41*, 1853−1859.
(6) Qin, S. H.; Oin, D. Q.; Ford, W. T.; Resasco, D. E.; Herrera, J. E. *J. Am. Chem. Soc.* **2004**, *126*, 170−176.
(7) Qin, S. H.; Qin, D. Q.; Ford, W. T.; Resasco, D. E.; Herrera, J. E. *Macromolecules* **2004**, *37*, 752−757.
(8) Qin, S. H.; Qin, D. Q.; Ford, W. T.; Herrera, J. E.; Resasco, D. E.; Bachilo, S. M.; Weisman, R. B. *Macromolecules* **2004**, *37*, 3965−3967.
(9) Hill, D. E.; Lin, Y.; Rao, A. M.; Allard, L. F.; Sun, Y. P. *Macromolecules* **2002**, *35*, 9466−9471.
(10) Viswanathan, G.; Chakrapani, N.; Yang, H. C.; Wei, B. Q.; Chung, H. S.; Cho, K. W.; Ryu, C. Y.; Ajayan, P. M. *J. Am. Chem. Soc.* **2003**, *125*, 9258−9259.
(11) Yao, Z.; Braidy, N.; Botton, G. A.; Adronov, A. *J. Am. Chem. Soc.* **2003**, *125*, 16015−16024.
(12) Liu, Y. Q.; Adronov, A. *Macromolecules* **2004**, *37*, 4755−4760.
(13) Sun, Y. P.; Fu, K. F.; Lin, Y.; Huang, W. J. *Acc. Chem. Res.* **2002**, *35*, 1096−1104.
(14) Kong, H.; Gao, C.; Yan, D. Y. *J. Am. Chem. Soc.* **2004**, *126*, 412−413.
(15) Riggs, J. E.; Guo, Z. X.; Carroll, D. L.; Sun, Y. P. *J. Am. Chem. Soc.* **2000**, *122*, 5879−5880.
(16) Sano, M.; Kamino, A.; Okamura, J.; Shinkai, S. *Langmuir* **2001**, *17*, 5125−5128.
(17) Wu, W.; Zhang, S.; Li, Y.; Li, J. X.; Liu, L. Q.; Qin, Y. J.; Guo, Z. X.; Dai, L. M.; Ye, C.; Zhu, D. B. *Macromolecules* **2003**, *36*, 6286−6288.
(18) Lin, Y.; Zhou, B.; Fernando, K. A. S.; Liu, P.; Allard, L. F.; Sun, Y. P. *Macromolecules* **2003**, *36*, 7199−7204.
(19) Krusic, P. J.; Wasserman, E.; Keizer, P. N.; Morton, J. R.; Preston, K. F. *Science* **1991**, *254*, 1183−1185.
(20) Krusic, P. J.; Wasserman, E.; Parkinson, B. A.; Malone, B.; Holler, E. R.; Keizer, P. N.; Morton, J. R.; Preston, K. F. *J. Am. Chem. Soc.* **1991**, *113*, 6274−6275.
(21) Peng, H. P.; Reverdy, P.; Khabashesku, V. N.; Margrave, J. L. *Chem. Commun.* **2003**, 362−363.
(22) Ying, Y. M.; Saini, R. K.; Liang, F.; Sadana, A. K.; Billups, W. E. *Org. Lett.* **2003**, *5*, 1471−1473.
(23) Shaffer, M. S. P.; Koziol, K. *Chem. Commun.* **2002**, 2074−2075.
(24) Barraza, H. J.; Pompeo, F.; O'Rear, E. A.; Resasco, D. E. *Nano Lett.* **2002**, *2*, 797−802.
(25) Audouin, F.; Nuffer, R.; Mathis, C. *J. Polym. Sci., Part A: Polym. Chem.* **2004**, *42*, 3456−3463.
(26) Audouin, F.; Nunige, S.; Nuffer, R.; Mathis, C. *Synth. Met.* **2001**, *121*, 1149−1150.
(27) Audouin, F.; Nuffer, R.; Mathis, C. *J. Polym. Sci., Part A: Polym. Chem.* **2004**, *42*, 4820−4829.
(28) Georges, M. K.; Veregin, R. P. N.; Kazmaier, P. M.; Hamer, G. K. *Macromolecules* **1993**, *26*, 2987−2988.
(29) Hawker, C. J.; Bosman, A. W.; Harth, E. *Chem. Rev.* **2001**, *101*, 3661−3688.
(30) Lohmeijer, B. G. G.; Schubert, U. S. *J. Polym. Sci., Part A: Polym. Chem.* **2004**, *42*, 4016−4027.
(31) Gopalan, P.; Li, X. F.; Li, M. Q.; Ober, C. K.; Gonzales, C. P.; Hawker, C. J. *J. Polym. Sci., Part A: Polym. Chem.* **2003**, *41*, 3640−3656.
(32) Benoit, D.; Chaplinski, V.; Braslau, R.; Hawker, C. J. *J. Am. Chem. Soc.* **1999**, *121*, 3904−3920.
(33) Malmstrom, E.; Miller, R. D.; Hawker, C. J. *Tetrahedron* **1997**, *53*, 15225−15236.
(34) Bahr, J. L.; Mickelson, E. T.; Bronikowski, M. J.; Smalley, R. E.; Tour, J. M. *Chem. Commun.* **2001**, 193−194.
(35) Bachilo, S. M.; Strano, M. S.; Kittrell, C.; Hauge, R. H.; Smalley, R. E.; Weisman, R. B. *Science* **2002**, *298*, 2361−2366.
(36) Strano, M. S.; Doorn, S. K.; Haroz, E. H.; Kittrell, C.; Hauge, R. H.; Smalley, R. E. *Nano Lett.* **2003**, *3*, 1091−1096.
(37) Huang, W. J.; Fernando, S.; Lin, Y.; Zhou, B.; Allard, L. F.; Sun, Y. P. *Langmuir* **2003**, *19*, 7084−7088.
(38) Banerjee, S.; Wong, S. S. *Nano Lett.*, in press.
(39) Chen, Z. F.; Thiel, W.; Hirsch, A. *ChemPhysChem* **2003**, *4*, 93.
(40) Jorio, A.; Souza, A. G.; Dresselhaus, G.; Dresselhaus, M. S.; Swan, A. K.; Unlu, M. S.; Goldberg, B. B.; Pimenta, M. A.; Hafner, J. H.; Lieber, C. M.; Saito, R. *Phys. Rev. B* **2002**, *65*, art. no.-155412.
(41) Ma, Q.; Wooley, K. L. *J. Polym. Sci., Part A: Polym. Chem.* **2000**, *38*, 4805−4820.
(42) Cahill, L. S.; Yao, Z.; Adronov, A.; Penner, J.; Moonoosawmy, K. R.; Kruse, P.; Goward, G. R. *J. Phys. Chem. B* **2004**, *108*, 11412−11418.

MA048273S